LANGMUIR

pubs.acs.org/Langmuir Article

# Membrane Binding Kinetics of Amphipathic Helical Peptides from Hepatitis C Virus: Quartz Crystal Microbalance with Dissipation Monitoring

*Published as part of Langmuir special issue "Highlighting Contributions from our Editorial Board Members in 2026".*

Young Hwan Choe, Enzo Ng, Vladmir P. Zhdanov, Dongping Jiang, and Nam-Joon Cho*

Cite This: *Langmuir* 2026, 42, 32381−32391 Read Online

ACCESS | Metrics & More | Article Recommendations | Supporting Information

**ABSTRACT:** Using quartz crystal microbalance with dissipation monitoring (QCM-D), we investigate the kinetics of attachment of three amphipathic helical (AH) peptides to a supported POPC lipid bilayer. The focus is on the peptides derived from hepatitis C virus (HCV) nonstructural proteins: the N-terminal AH of NS5A and two helices (AH1 and AH2) from NS4B. NS5A AH exhibits conventional monotopic insertion with rapid frequency decrease, minimal dissipation increase, and immediate stabilization, indicating rigid interfacial embedding and bilayer immobilization without formation of a viscoelastic overlayer. NS4B AH1 displays monotonic adsorption similar to NS5A but with moderately elevated dissipation, consistent with cooperative lateral peptide−peptide interactions superimposed on membrane insertion. In contrast, NS4B AH2 shows strongly non-Langmuirian behavior. At low concentrations (3.25−6.5 $\mu$M), it forms a highly dissipative, hydrated interfacial layer dominated by peptide aggregation. Above a threshold at 6.5 $\mu$M, there is transition toward a compact membrane-engaged state with reduced dissipation and late-stage structural relaxation. This aggregation-to-insertion transition reflects a shift in dominant interaction from lateral self-association to cooperative membrane coupling. These observations have been interpreted by employing a phenomenological kinetic model implying three peptide surface states representing disordered aggregates and compact membrane-bound domains.

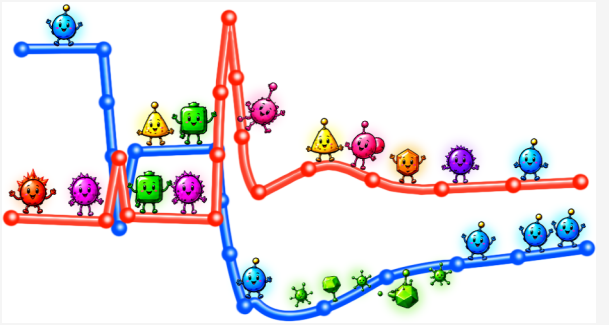

## INTRODUCTION

Adsorption of large biomolecules is of interest from various perspectives. In this context, the best example is adsorption of proteins which can be tracked over decades.[1−3] The corresponding literature is extremely extensive, and many recent studies have been performed by using QCM-D (see, e.g., references in the Supporting Information). Much less attention has been paid to adsorption of peptides at various surfaces in general (see, e.g., experiments[4−8] and theoretical studies[9,10]) and especially at lipid bilayers (see, e.g., refs 11 and 12). Herein, we focus on amphipathic $\alpha$-helices from HCV. In nature, such helical peptides are found as terminal fragments of proteins. Their role there is to regulate the interaction of proteins with a lipid bilayer via suitable hydrophobic and polar residues. Unlike transmembrane species, these helices interact more softly with lipid bilayers, inserting shallowly into a single leaflet while remaining peripherally bound.[4,12] Despite their simplicity, such helices can access a broad spectrum of interfacial behavior,[13] including curvature generation,[14,15] membrane stiffening,[16,17] lipid demixing,[18,19] and cooperative assembly.[20,21] The extent to which primary sequence variations modulate the thermodynamic landscape of adsorption of such peptides at a membrane and the specifics of the corresponding kinetics remain, however, incompletely understood.

A defining feature of the HCV replication strategy is the extensive remodeling of host endoplasmic reticulum membranes into a specialized replication organelle, often referred to as the membranous web.[22] Central to this process are the nonstructural proteins NS4B and NS5A, both of which exhibit strong membrane affinity (Figure 1) and play distinct but coordinated roles in replication complex formation.[23] NS4B topology includes several hydrophobic segments that span the lipid bilayer, as well as cytosolic regions that contain amphipathic helices[23,24] that could induce curvature stresses

Received: May 10, 2026
Revised: September 4, 2026
Accepted: September 4, 2026
Published: September 28, 2026



Downloaded from pubs.acs.org/langd5/article-pdf/42/44/32381/6860487/acs.langmuir.6c02775.pdf by NANYANG TECHNOLOGICAL UNIV user on 19 November 2026


© 2026 American Chemical Society

https://doi.org/10.1021/acs.langmuir.6c02775
*Langmuir* 2026, 42, 32381−32391

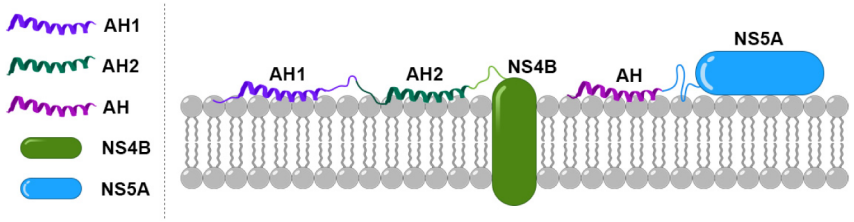


**Figure 1.** Scheme of membrane association of hepatitis C virus (HCV) proteins, NS4B and NS5A, as inferred from the structural and biochemical studies of refs [23,24,27,28]. NS4B is depicted as an integral membrane protein containing multiple transmembrane domains, while NS5A is shown as a peripheral membrane-associated protein anchored via its N-terminal amphipathic helix (AH).

and facilitate membrane rearrangement.[25,26] In contrast, NS5A is not a transmembrane protein. Structural studies have shown that NS5A forms a stable $\alpha$-helical conformation with distinct hydrophobic and polar faces. This enables selective interaction with lipid headgroups and acyl chains to associate peripherally at membranes instead.[27,28] This mode of membrane binding is crucial for NS5A's role in RNA replication, lipid metabolism modulation, and interaction with host factors. Despite their relatively short sequences, these helices encode distinct physicochemical properties, including local hydrophobicity, charge distribution, and conformational flexibility, which ultimately govern their adsorption kinetics and membrane interaction mechanisms to exhibit diverse behaviors ranging from rigid monotopic insertion to dynamic, cooperative assembly at membrane interfaces.[29,30]

By analogy with proteins,[1−3] adsorption of amphipathic helices onto lipid bilayers is a coupled transport-attachment-reorganization process. Molecules diffuse from bulk solution toward an interface, undergo initial attachment, and subsequently explore lateral configurations through surface diffusion and conformational rearrangement.[31,32] In the simplest cases, adsorption follows a Langmuirian regime in which the surface is progressively occupied until saturation by a quasi-monolayer of attached helices.[33] In more complex regimes, lateral peptide−peptide interactions,[12,33] domain formation,[34−37] or structural relaxation[38,39] within the interfacial layer can lead to non-Langmuirian kinetics and thickness evolution reminiscent of nonequilibrium film growth.[40] Such behavior parallels protein adsorption accompanied by denaturation,[41] aggregation-driven protein multilayer formation[42] and, to some extent, phenomena described in molecular-beam epitaxy.[43] Yet, quantitative kinetic descriptions tailored to short amphipathic helices remain largely undeveloped.

Lipid bilayers introduce additional complexity relative to rigid substrates. The interface is fluid, deformable, and capable of accommodating insertion-driven stress.[44] Disentangling insertion-dominant behavior from aggregation-dominant interfacial assembly requires simultaneous resolution of mass uptake and mechanical response which can be precisely achieved through the QCM-D. By tracking both frequency shifts ($\Delta F$) and energy dissipation changes ($\Delta D$), it allows one to distinguish rigid interfacial embedding from formation of hydrated, viscoelastic overlayers.[45,46] A low $\Delta D/(-\Delta F)$ ratio indicates compact, mechanically coupled insertion, whereas elevated dissipation signals the presence of compliant, water-rich interfacial structures.[47,48] The coupled evolution of $\Delta F$ and $\Delta D$ therefore encodes mechanistic information about adsorption regime, aggregation state, and structural relaxation.

Herein, we exploit the QCM-D technique to interrogate the membrane binding dynamics of three amphipathic helical peptides under consideration. Although these peptides share canonical amphipathic topology, their sequences differ in hydrophobic moment, aromatic anchoring content, and charge distribution.[49] We hypothesized that these differences encode distinct regimes of adsorption on fluid lipid bilayers. To interpret the experiments, we employ a phenomenological kinetic model implying the formation and interplay of disordered aggregates and compact membrane-engaged domains.

## MATERIALS AND METHODS

### Materials

1-Palmitoyl-2-oleoyl-*sn*-glycero-3-phosphocholine (POPC) was purchased from Avanti Polar Lipids and used without further purification. Chloroform (HPLC-grade), phosphate-buffered saline (PBS, pH 7.4), and sodium chloride (NaCl) were obtained from Sigma-Aldrich. Ultrapure water (18.2 MΩ·cm) was produced using a Milli-Q system.

Synthetic peptides corresponding to the amphipathic helices of HCV nonstructural proteins were obtained from GenScript Biotech Corporation with purity >95%. The sequences included: (i) NS5A AH (27-mer, SGSWLRVWDICTVLTDFKTWLQSKL), (ii) NS4B AH1 (ASHLPYIEQGMQLAEQFQKALGLLQ), and (iii) NS4B AH2 (WRTLEAFWAKHMWNFISGIQYLA). Peptide hydrophobicity and bilayer partitioning was examined with using the Wimley-White interfacial hydrophobicity scale[50] via Membrane Protein Explorer (MPEx).[51] Peptide secondary structure was predicted employing the Network Protein Sequence Analysis (NPSA)[52] webtool, via the following methods: DSC, HNNC, MLRC, PHD, SOPM, and Sec. Cons.

Peptides were dissolved in PBS and stored at −20 °C prior to use. Working solutions were freshly prepared at concentrations ranging from 3.25 $\mu$M to 26 $\mu$M.

### Preparation of Vesicles

POPC vesicles were prepared using a standard thin-film hydration and extrusion method.[53] Briefly, POPC dissolved in chloroform was dried under a gentle nitrogen stream to form a lipid film, followed by vacuum desiccation overnight to remove residual solvent. The lipid film was rehydrated in PBS buffer (10 mM phosphate, 150 mM NaCl, pH 7.4) to a final concentration of 5 mg mL$^{-1}$.

The resulting vesicles were subjected to repeated extrusion employing a Mini Extruder (Avanti Polar Lipids) through polycarbonate membranes with pore sizes of 50 nm followed by 30 nm. The final vesicle size distribution was confirmed by dynamic light scattering (DLS) to be approximately 60 ± 5 nm. Vesicles were used within 48 h of preparation.

### Formation of Supported Lipid Bilayers

Supported lipid bilayers (SLBs) were formed on QCM-D sensors ($SiO_2$-coated) which were cleaned by sequential rinsing with ethanol and water, followed by UV/ozone treatment for 15 min to remove organic contaminants and enhance surface hydrophilicity.

Small unilamellar vesicle (SUV) solution (0.05 mg mL$^{-1}$ in PBS) was introduced into the QCM-D flow module at a flow rate of 50 $\mu$L min$^{-1}$. Vesicle adsorption and spontaneous rupture led to the

Downloaded from pubs.acs.org/langd5/article-pdf/42/44/32381/6860487/acs.langmuir.6c02775.pdf by NANYANG TECHNOLOGICAL UNIV user on 19 November 2026


https://doi.org/10.1021/acs.langmuir.6c02775
Langmuir 2026, 42, 32381−32391

formation of a continuous POPC bilayer that was confirmed by a characteristic frequency shift ($\Delta F \approx -25$ to $-27$ Hz) and minimal dissipation ($\Delta D < 0.5 \times 10^{-6}$),[54,55] consistent with a rigid, homogeneous membrane.

Following bilayer formation, the system was rinsed with PBS buffer until a stable baseline was achieved.

### Quartz Crystal Microbalance with Dissipation Monitoring (QCM-D)

QCM-D measurements were performed using a Q-Sense E4 instrument (Biolin Scientific AB, Gothenburg, Sweden). Silica-coated quartz sensors with a fundamental frequency of 5 MHz were used. All experiments were conducted at 25 °C under continuous flow conditions. Frequency ($\Delta F$) and dissipation ($\Delta D$) shifts were recorded simultaneously at multiple overtones ($n$ = 3, 5, 7, 9, 11, and 13). The normalized frequency ($\Delta F/n$) was used for analysis.

After establishing a stable bilayer baseline, peptide solutions at defined concentrations (3.25, 6.5, 13, and 26 $\mu$M) were injected into the flow chamber at 50 $\mu$L min$^{-1}$. Peptide−membrane interaction was monitored in real time until equilibrium or steady-state behavior was reached. Subsequently, PBS buffer was reintroduced to remove loosely bound peptides and assess the reversibility and stability of membrane association.

### Viscoelastic Modeling

To extract quantitative information on interfacial properties, QCM-D data were analyzed using a Voigt−Voinova viscoelastic model,[56] operating with the effective thickness ($t$), shear viscosity ($\eta$), and shear modulus ($\mu$). For rigid layers exhibiting low dissipation ($\Delta D < 1 \times 10^{-6}$), the Sauerbrey equation was applied to estimate mass changes:[57] $\Delta m = -C \times (\Delta F/n)$, where $C$ = 17.7 ng cm$^{-2}$ Hz$^{-1}$. For viscoelastic layers, multi-overtone fitting was performed using commercial software (Q-Tools, Q-Sense AB), assuming constant density and frequency-independent viscosity. The model allowed the determination of coupled mass (including hydrodynamically trapped solvent) and differentiation between rigid insertion and hydrated, dissipative interfacial structures.[46]

### Data Analysis and Kinetic Modeling

The adsorption behavior of each peptide was evaluated by analyzing the coupled evolution of $\Delta F$ and $\Delta D$. The ratio $\Delta D/(-\Delta F)$ was used as a qualitative indicator of interfacial viscoelasticity, where low values correspond to rigid membrane insertion and high values indicate the formation of hydrated, soft layers.[45]

For NS4B AH2, a phenomenological kinetic model was implemented to describe the coexistence of three interfacial states including disordered peptide aggregates and compact membrane-bound domains of two types. The model incorporates adsorption, lateral aggregation, and structural relaxation processes, enabling reproduction of concentration-dependent $\Delta F-\Delta D$ trajectories.

## RESULTS AND DISCUSSION

### Predicted Amphipathic Architecture of HCV-Derived Amphipathic Helices

Amphipathic helices represent one of the most fundamental structural motifs by which peripheral and monotopic proteins interact with biological membranes.[13] Their functionality arises from the spatial segregation of hydrophobic and hydrophilic residues along the helical axis, generating a directional hydrophobic moment that drives preferential partitioning into membrane interfaces.[4] To quantify and visualize these features, helical wheel projections are commonly used to map residue distribution and infer membrane binding propensity.[58,59]

The three peptides examined here—NS5A AH, NS4B AH1, and NS4B AH2—exhibit markedly different amphipathic architectures despite their shared classification as membrane-active helices. The NS5A amphipathic helix displays a canonical organization, with a continuous hydrophobic face composed primarily of leucine, tryptophan, and valine residues, opposed by a polar and charged face enriched in lysine and aspartate. Structural and NMR studies have previously demonstrated that the NS5A N-terminal helix adopts a well-defined $\alpha$-helical conformation upon membrane association, functioning as a robust membrane anchor.[27]

In contrast, NS4B AH1 presents a less sharply defined amphipathic segregation. The distribution of polar and charged residues is more dispersed, and the hydrophobic face is comparatively interrupted. Such characteristics are often associated with helices that participate in cooperative or transient interactions, where peptide−peptide interactions or local lipid rearrangements play a more prominent role than simple insertion energetics.[29]

NS4B AH2 exhibits yet another distinct profile, characterized by a strong clustering of hydrophobic residues, including aromatic amino acids such as tryptophan and phenylalanine.[23,24] This creates an extended hydrophobic part that may promote deeper insertion into the lipid bilayer or facilitate self-association at the membrane interface.[23,24] Aromatic residues are known to preferentially localize at membrane interfaces due to favorable interactions with lipid headgroups and acyl chains, often stabilizing interfacial binding and influencing membrane curvature.[50,60]

Circular dichroism spectroscopy provides complementary insight into the conformational behavior of these peptides in different environments.[61] In aqueous solution, all three peptides exhibit reduced helicity, reflecting conformational flexibility and the absence of stabilizing hydrophobic interactions. This is consistent with the general behavior of amphipathic helices, which often remain partially disordered in solution and adopt structured conformations only upon encountering a membrane-like environment.

The addition of trifluoroethanol, a helix-promoting co-solvent, induces pronounced $\alpha$-helical signatures in all peptides, as evidenced by the characteristic double minima near 209 and 222 nm. This confirms that each sequence possesses an intrinsic propensity to form $\alpha$-helices, even if this structure is not fully realized in aqueous conditions. Importantly, in the presence of POPC vesicles,[62] all peptides show increased $\alpha$-helicity relative to water, demonstrating membrane-induced folding. This phenomenon is a hallmark of amphipathic helices and reflects the coupling between membrane binding and secondary structure formation. However, the extent and stability of this folding differ between peptides, consistent with their distinct amphipathic architectures. NS5A AH likely undergoes rapid and stable helix formation upon binding, whereas NS4B-derived helices may exhibit more complex folding dynamics that depend on peptide concentration, lipid composition, and interfacial crowding.

### Secondary Structure Stabilization and Residue-Resolved Interfacial Energetics of HCV Amphipathic Helical Peptides

Understanding membrane association of amphipathic helices requires not only structural characterization but also quantitative assessment of residue-level energetics that govern interfacial partitioning.[4,23,24] The Wimley−White interfacial hydrophobicity scale provides one of the most widely accepted thermodynamic frameworks for this purpose, as it directly measures the free energy associated with transferring individual

Downloaded from pubs.acs.org/langds/article-pdf/42/44/32381/6860487/acs.langmuir.6c02775.pdf by NANYANG TECHNOLOGICAL UNIV user on 19 November 2026



https://doi.org/10.1021/acs.langmuir.6c02775
Langmuir 2026, 42, 32381−32391

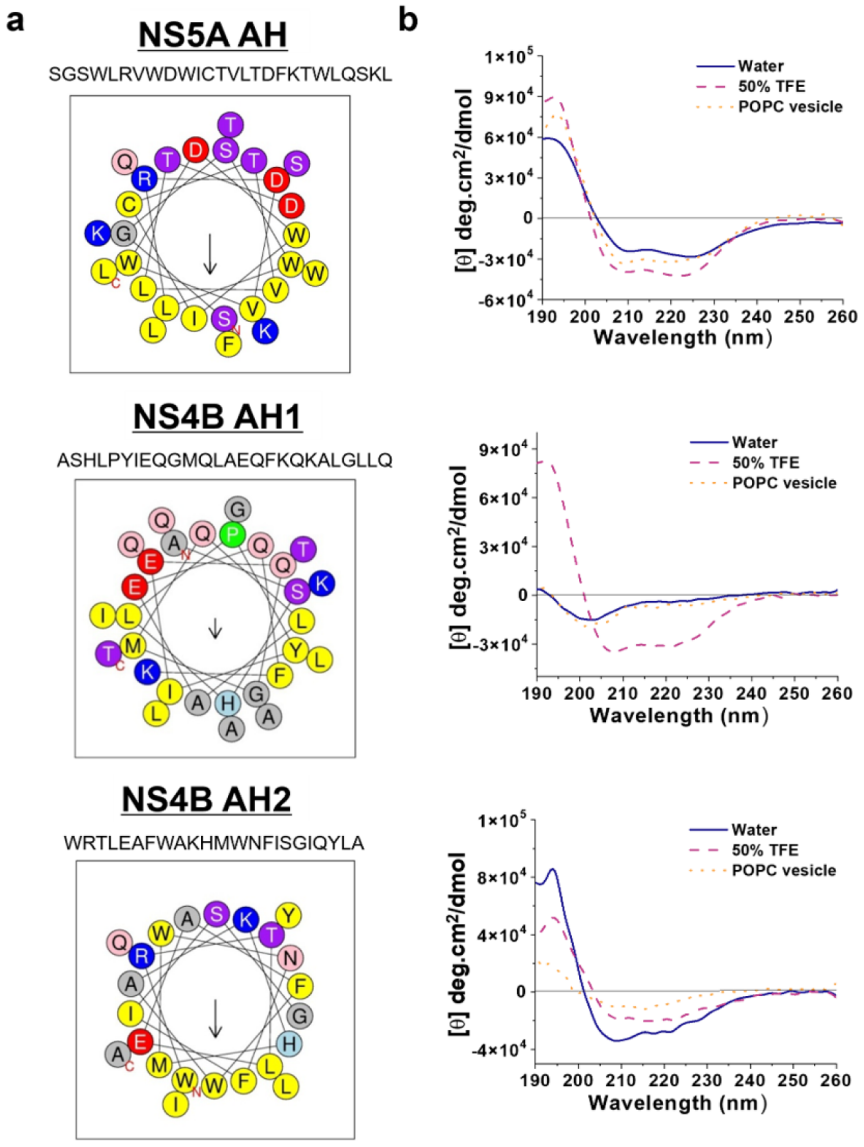


**Figure 2.** Amphipathic architecture and secondary structure of HCV-derived helices NS5A AH, NS4B AH1, and NS4B AH2. (a) Helical wheel projections of the amphipathic helices derived from HCV. Residues are color-coded: hydrophobic (yellow), polar uncharged (gray), positively charged (blue), and negatively charged (red). The projections reveal the spatial arrangement of hydrophobic and polar residues, highlighting the amphipathic nature of each peptide. (b) Circular dichroism (CD) spectra measured under three conditions: aqueous buffer (water), 50% trifluoroethanol (TFE), and in the presence of POPC vesicles. In water and with POPC vesicles, NS4B AH1 and NS4B AH2 lack the canonical $\alpha$-helical double minima (~209 and ~222 nm). In TFE, characteristic $\alpha$-helical double minima at approximately 209 and 222 nm are observed, confirming helix-forming propensity.

amino acids from water into the membrane interface rather than the bilayer core.[50,63] The residue-resolved profiles shown here reveal that all three HCV-derived helices encode a nonrandom energetic landscape that strongly favors interfacial localization. For NS5A AH, the energetic profile exhibits a pronounced clustering of residues with positive interfacial preference, particularly in regions enriched with bulky hydrophobic and aromatic amino acids such as tryptophan, leucine, and valine. These residues contribute disproportionately to membrane affinity due to favorable interactions with both lipid acyl chains and interfacial headgroup regions. Aromatic residues, in particular, are known to act as interfacial anchors, stabilizing peptide positioning through cation–$\pi$ interactions and partial insertion into the bilayer.[60,64]

The red bars marking the predicted anchoring segments shown in the panels of Figure 3a correspond to a contiguous stretch of residues exhibiting favorable interfacial energetics. These segments align closely with the hydrophobic faces identified in the helical wheel projections (Figure 2), reinforcing the concept that amphipathicity is not only a geometric property but also an energetic one encoded at the sequence level. In contrast, NS4B AH1 displays a more heterogeneous energetic distribution, with alternating regions of favorable and less favorable interfacial residues. This fragmented profile implies weaker cooperative stabilization and may underlie its more dynamic or cooperative membrane interaction behavior. Such variability can promote transient exposure of polar residues or facilitate lateral peptide–peptide interactions, contributing to intermediate viscoelastic properties observed experimentally.

NS4B AH2 exhibits a distinct energetic signature characterized by a sharp transition from unfavorable to highly


https://doi.org/10.1021/acs.langmuir.6c02775
Langmuir 2026, 42, 32381−32391

Downloaded from pubs.acs.org/langds/article-pdf/42/44/32381/6860487/acs.langmuir.6c02775.pdf by NANYANG TECHNOLOGICAL UNIV user on 19 November 2026

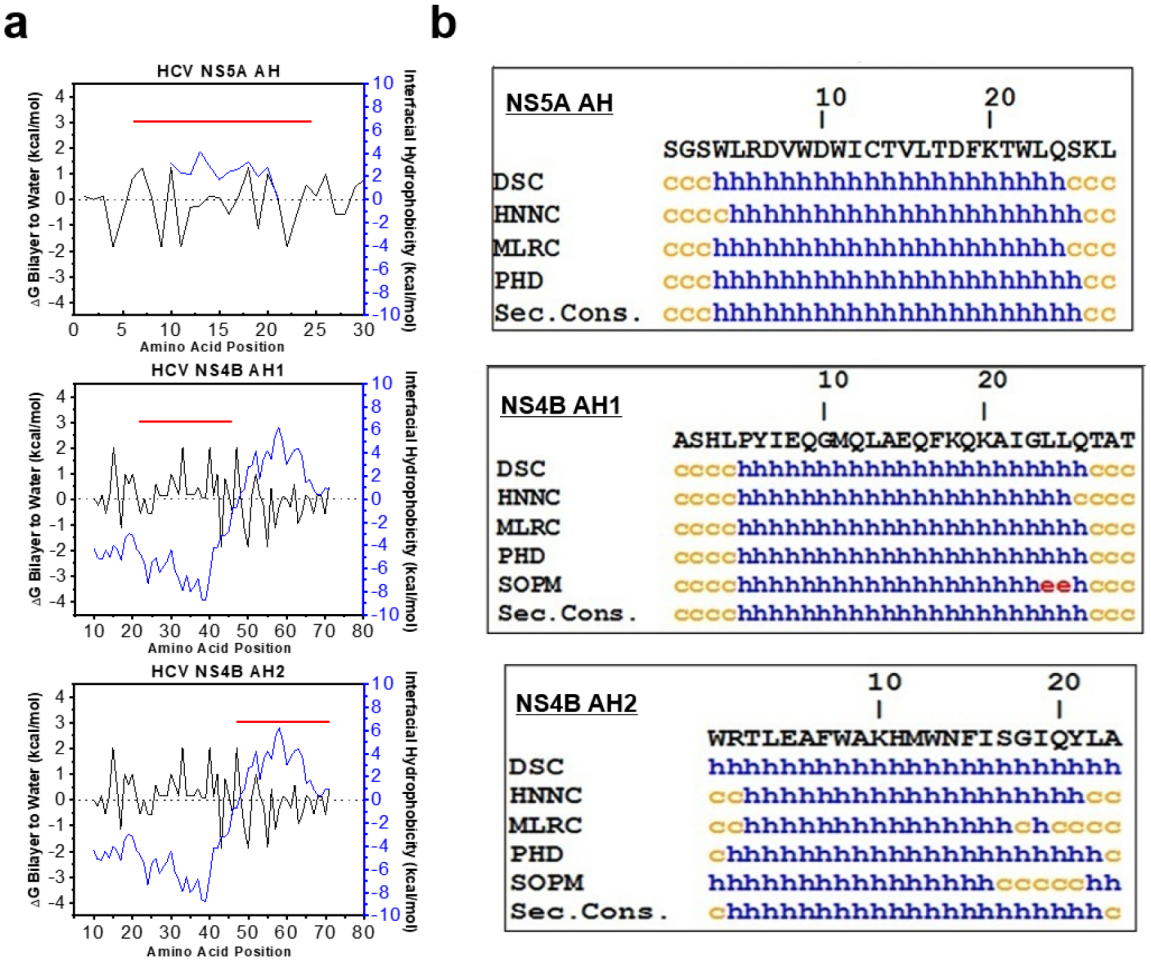


**Figure 3.** Residue-resolved interfacial energetics and secondary structure propensity of HCV NS5A AH, NS4B AH1, and NS4B AH2 (genotype 1b). (a) Residue-resolved energetic profiles calculated using the Wimley–White interfacial hydrophobicity scale. The left *y*-axis (black) represents the Gibbs free energy change. Positive values indicate thermodynamic favorability for the lipid membrane interface over water. The right *y*-axis (blue) represents interfacial hydrophobicity, reflecting the energetic preference for partitioning into the membrane interface. The horizontal red bar indicates a predicted amphipathic, membrane-anchoring segment. (b) Secondary structure predictions generated using multiple algorithms from the NPSA platform (DSC, HNNC, MLRC, PHD, SOPM, and consensus prediction). Predicted $\alpha$-helical regions were consistently identified, with strong agreement in the central segments.

favorable interfacial residues along the sequence. This gradient-like profile suggests the possibility of directional insertion or asymmetric membrane engagement. The presence of multiple aromatic residues further enhances its potential for strong interfacial anchoring, but the nonuniform distribution may also promote aggregation or concentration-dependent structural rearrangements at the membrane surface.

Complementing the energetic analysis, secondary structure predictions provide insight into the intrinsic folding propensity of these sequences (Figure 3b). Across all prediction algorithms used (DSC, HNNC, MLRC, PHD, SOPM), there is strong consensus that the central regions of each peptide adopt $\alpha$-helical conformations. This agreement among independent methods increases confidence in the structural assignment, as different algorithms rely on distinct statistical and machine learning approaches.[52]

The predicted helicity aligns well with the experimental CD data (Figure 2), supporting a model in which these peptides are predisposed to form $\alpha$-helices but require a membrane-like environment for full stabilization. This behavior is consistent with the concept of "coupled folding and binding," where secondary structure formation is energetically linked to membrane association.[65]

An important observation is that the amphipathic character and helical propensity of the NS5A AH are highly conserved across HCV genotypes, indicating strong evolutionary pressure to maintain this membrane binding function. Such conservation underscores the functional importance of precise interfacial energetics in viral replication. Even subtle perturbations in residue composition could disrupt membrane affinity, replication complex assembly, or protein–lipid interactions.

From a mechanistic perspective, the integration of residue-level energetics with secondary structure prediction provides a predictive framework for understanding membrane interaction behavior. Sequences with continuous regions of favorable interfacial energy and strong helical propensity are expected to exhibit stable, monotopic insertion. In contrast, sequences with heterogeneous energetics may display cooperative, concentration-dependent, or aggregation-prone behavior. These distinctions directly underline the kinetic regimes observed in QCM-D measurements, where NS5A AH behaves as a rigid


https://doi.org/10.1021/acs.langmuir.6c02775
Langmuir 2026, 42, 32381–32391

Downloaded from pubs.acs.org/langds/article-pdf/42/44/32381/6860487/acs.langmuir.6c02775.pdf by NANYANG TECHNOLOGICAL UNIV user on 19 November 2026

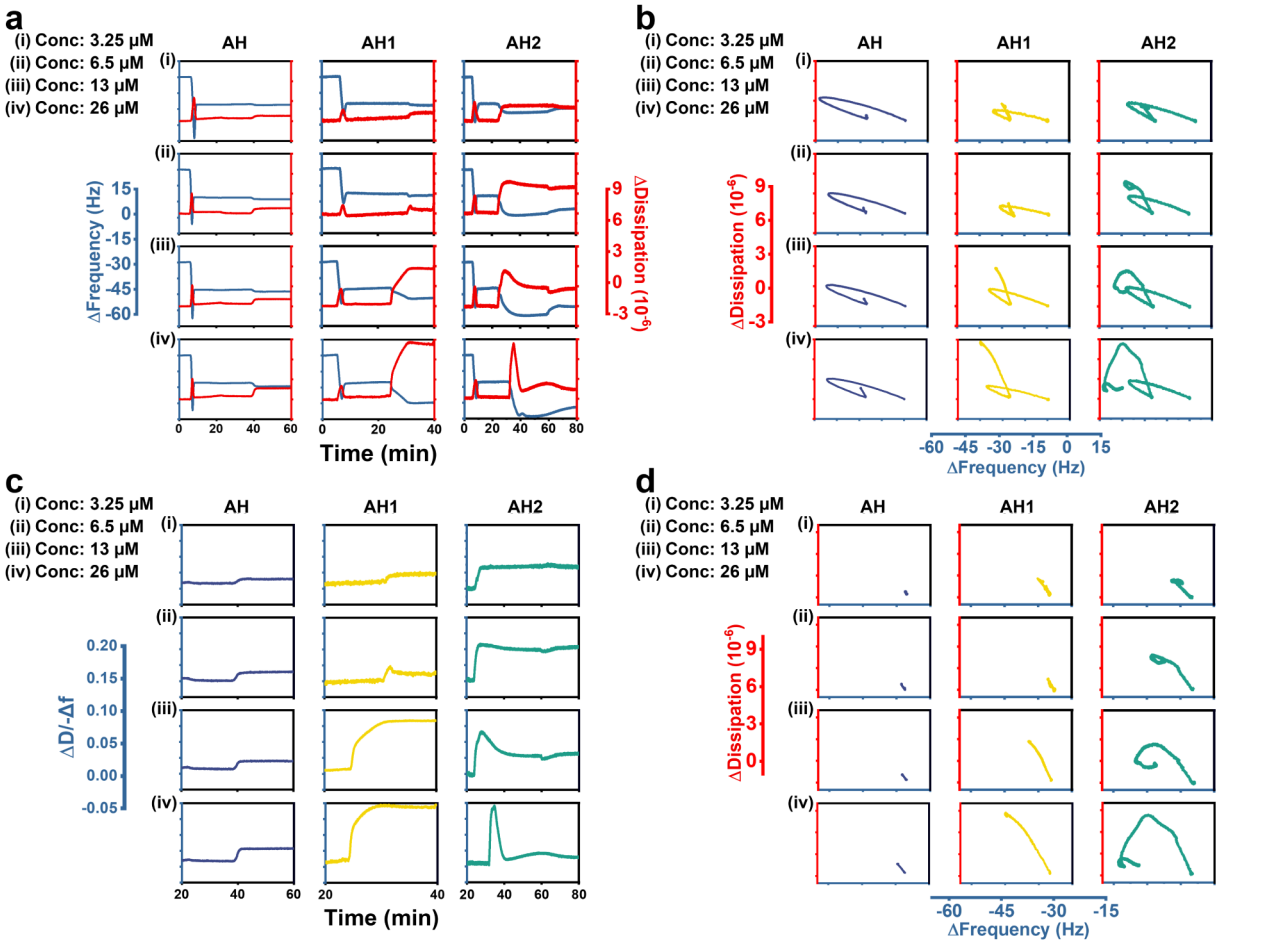


**Figure 4.** Concentration-dependent QCM-D adsorption kinetics of HCV-derived amphipathic helices on supported POPC lipid bilayers reveal distinct membrane interaction regimes. (a) Representative QCM-D sensorgrams show frequency ($\Delta F$, blue) and dissipation ($\Delta D$, red) responses of the fifth overtone during the interaction of NS5A AH, NS4B AH1, and NS4B AH2 peptides with supported POPC lipid bilayers. Supported lipid bilayers were first formed on $SiO_2$-coated quartz sensors prior to peptide injection. Peptides were then introduced at four concentrations: (i) 3.25 $\mu$M, (ii) 6.5 $\mu$M, (iii) 13 $\mu$M, and (iv) 26 $\mu$M. Following adsorption, the system was rinsed with buffer to stabilize the interfacial layer. Blue traces represent normalized frequency shifts ($\Delta F$), which primarily reflect changes in adsorbed mass and interfacial coupling, while red traces represent dissipation shifts ($\Delta D$), which indicate changes in viscoelasticity and structural rearrangement of the interfacial layer. (b) $\Delta F-\Delta D$ plots of the adsorption data from (a). (c) $\Delta D/(-\Delta F)$ ratio over time from 20 mins, highlighting peptide-bilayer interactions. Larger values of $\Delta D/(-\Delta F)$ indicate greater viscoelastic behavior. (d) $\Delta F-\Delta D$ plots from the same time period as (c), to highlight peptide-bilayer interactions.

inserter, while NS4B-derived helices show more complex interfacial dynamics.

## Adsorption Kinetics of NS5A AH, NS4B AH1, and NS4B AH2 on Supported POPC Lipid Bilayers

To investigate how sequence variation influences membrane adsorption behavior, QCM-D was used to monitor the interaction of NS5A AH, NS4B AH1, and NS4B AH2 peptides with supported POPC lipid bilayers over a concentration range of 3.25−26 $\mu$M (Figure 4a). Changes in resonance frequency ($\Delta F$) were employed to monitor mass adsorption and interfacial coupling, while dissipation shifts ($\Delta D$) provided insight into the viscoelastic properties and structural evolution of the adsorbed peptide layer. $\Delta F-\Delta D$ plots (Figure 4b and Figure 4d) were used to fingerprint the peptide−membrane interactions as previously reported.[47,66] NS5A AH exhibited highly reproducible monotonic adsorption behavior across the entire concentration range. Upon peptide injection, a rapid decrease in $\Delta F$ was consistently observed, indicating immediate peptide adsorption onto the supported lipid bilayer. This response was accompanied by only minimal increases in $\Delta D$, resulting in a persistently low $\Delta D/(-\Delta F)$ ratio (Figure 4c). Following adsorption, both signals rapidly stabilized without secondary transitions, delayed restructuring, or signal drift during subsequent buffer exchange. Similarly, a dense, linear $\Delta F-\Delta D$ plot was obtained. The low dissipation response suggests that NS5A AH forms a rigid and tightly coupled interfacial layer rather than a hydrated viscoelastic assembly. Previous structural studies have shown that NS5A amphipathic helices associate with membranes through shallow insertion of hydrophobic residues into the acyl chain region while polar residues remain solvent exposed, thereby anchoring the protein to intracellular membranes without inducing major membrane disruption.[67] The absence of concentration-dependent kinetic transitions further suggests that membrane insertion remains the dominant interaction pathway even at elevated surface coverage, although the weak concentration dependence is equally consistent with near saturation of the accessible binding sites already at the lowest concentration studied.

NS4B AH1 displayed similarly monotonic adsorption kinetics but generated consistently higher dissipation responses


https://doi.org/10.1021/acs.langmuir.6c02775
Langmuir 2026, 42, 32381−32391

Downloaded from pubs.acs.org/langds/article-pdf/42/44/32381/6860487/acs.langmuir.6c02775.pdf by NANYANG TECHNOLOGICAL UNIV user on 19 November 2026

compared with NS5A AH. At all concentrations, $\Delta F$ decreased continuously following peptide injection, indicating efficient membrane association. However, the larger $\Delta D$ response suggests that AH1 forms a less rigid interfacial layer. A mostly linear $\Delta F-\Delta D$ plot was obtained, hinting at a similar adsorption mechanism to NS5A AH. However, unlike NS5A AH, AH1 appears to undergo primary membrane insertion accompanied by cooperative lateral peptide−peptide interactions within the membrane plane. This interpretation is based on the higher $\Delta D/(-\Delta F)$ ratio of AH1 relative to NS5A AH at comparable mass uptake, which indicates a softer, less rigidly coupled overlayer than rigid insertion alone would produce. As surface coverage increases, lateral clustering likely generates local heterogeneity in membrane packing, resulting in moderate viscoelastic dissipation. Such cooperative assembly behavior may be particularly relevant to the biological function of NS4B, which plays a central role in generating HCV replication organelles through membrane remodeling and curvature stabilization.[68,69] Compared with NS5A AH, AH1 therefore appears to balance stable insertion with modest collective assembly behavior.

In contrast, NS4B AH2 exhibited fundamentally different adsorption kinetics characterized by strong concentration dependence and pronounced nonmonotonic behavior. At lower concentrations (3.25−6.5 $\mu$M), adsorption generated relatively modest frequency shifts but disproportionately large increases in dissipation. The resulting high $\Delta D/(-\Delta F)$ ratio indicates formation of a soft, hydrated, and weakly coupled interfacial layer. In this low-concentration regime, peptide−peptide interactions appear to dominate over peptide-lipid interactions. The basis for this assignment is the high $\Delta D/(-\Delta F)$ ratio itself, which is the QCM-D signature of a soft, hydrated layer rather than of compact membrane insertion; it contrasts with the low $\Delta D/(-\Delta F)$ of NS5A AH (rigid insertion) and the intermediate $\Delta D/(-\Delta F)$ of AH1 (insertion with moderate lateral association). The soft, hydrated AH2 layer is consistent with loosely associated peptide aggregates, in line with the strongly clustered hydrophobic and aromatic residues of the AH2 sequence (Sections −Sections), which favor self-association.

A distinct transition emerged between 6.5 and 13 $\mu$M. At 13 $\mu$M, both $\Delta F$ and $\Delta D$ deviated from the proportional scaling observed at lower concentrations, indicating structural reorganization within the adsorbed layer. At 26 $\mu$M, AH2 produced a dramatic transient increase in dissipation followed by substantial frequency decreases and subsequent relaxation. A spiral $\Delta F-\Delta D$ plot was obtained which suggests that the initially formed soft aggregate layer undergoes structural compaction and transitions into a more tightly membrane-coupled state. The reduction in $\Delta D/(-\Delta F)$ ratio at higher concentrations supports a shift from aggregation-dominated adsorption toward insertion-dominated membrane engagement. The behavior of AH2 is particularly significant because it demonstrates that minor sequence differences among amphipathic helices can generate fundamentally different interfacial free-energy landscapes. Whereas NS5A AH follows a rigid insertion pathway and AH1 follows a cooperative insertion pathway, AH2 appears to undergo a multistate adsorption process involving initial aggregation, structural reorganization, and subsequent membrane insertion. These findings suggest that HCV amphipathic helices may encode distinct membrane remodeling functions through sequence-dependent control of interfacial kinetics.

## Mean-Field Peptide Adsorption Kinetics

For interpretation of the QCM-D-measured kinetics of adsorption and structural relaxation of NS5A AH, NS4B AH1, and NS4B AH2 at a lipid bilayer, it is instructive to examine kinetic models of protein adsorption to identify a suitable model to be adapted for the context under consideration. One of the key two-state models implies that right after adsorption, proteins are in state 1 which is close to the compact native state. Following which there is a transition to the altered (denatured) state 2 with a larger contact area with the support.[1,2] The corresponding kinetics depend on whether one admits desorption. Our experimental results indicate that the changes of the state of the adsorbed peptide overlayer after rinsing is nearly negligible, and accordingly the peptide desorption does not appear to play a role. Without desorption, the two-state model is able to describe one of the key features of the observed kinetics of the peptides under considerations, namely, the increase of the final peptide uptake (tracked by $\Delta F$) with increasing peptide concentration in solution but it does not reproduce the drop of $\Delta D$ after reaching the maximum in the most interesting case of AH2 (Figure 4a). To describe this feature, two three-state models were used (described in detail in Supporting Information).

Compared to the two-state model or available three-state models,[1,2] the models under consideration imply a more complex mechanism of peptide relaxation in state 1. In both models, the peptide transition from state 1 to state 2 occurs provided there is empty space in the adsorbed overlayer (as in the two-state model). In addition, there is slower transition to state 3 without the change of contact area such that empty space is not required. The latter transition is considered monomolecular in the first model and bimolecular in the second model. The first model is found to be more suitable (see the comparison of the corresponding kinetics in Supporting Information).

Focusing here on the first three-state model, we note that the corresponding mean-field kinetic equations can be represented in terms of the surface concentrations of peptide in states 1, 2, and 3, $c_1$, $c_2$, and $c_3$, and/or coverages, $\theta_1$, $\theta_2$, and $\theta_3$, related as

$$\theta_1 = s_1 c_1, \quad \theta_2 = s_2 c_2, \quad \text{and } \theta_3 = s_3 c_3 \tag{1}$$

where $s_1$, $s_2$ ($>s_1$), and $s_3$ ($=s_1$) are the corresponding contact areas. The equations for concentrations are physically more transparent, whereas the equations for coverages are more convenient for calculations (see the Supporting Information). In terms of coverages, the equations are as follows

$$\begin{aligned} d\theta_1/dt &= k_a c - k_{12}(1-\theta)\theta_1 - k_{13}\theta_1, \\ d\theta_2/dt &= \alpha k_{12}(1-\theta)\theta_1, \\ d\theta_3/dt &= k_{13}\theta_1 \end{aligned} \tag{2}$$

where $c$ is the peptide concentration in solution, $\theta = \theta_1 + \theta_2 + \theta_3$ is the total coverage, $k_a$ is the coverage-dependent adsorption rate constant (eq 3 below), $k_{12}$ and $k_{13}$ are the relaxation rate constants, and $\alpha \equiv s_2/s_1 > 1$ is the coefficient taking into account that the transition to state 2 is accompanied by increase of the contact area.

Under the flow conditions employed in QCM-D measurements, adsorption is diffusion-limited and independent of coverage almost up to saturation,[70] and the coverage-dependent attachment rate constant can be expressed as

Downloaded from pubs.acs.org/langds/article-pdf/42/44/32381/6860487/acs.langmuir.6c02775.pdf by NANYANG TECHNOLOGICAL UNIV user on 19 November 2026



https://doi.org/10.1021/acs.langmuir.6c02775
Langmuir 2026, 42, 32381−32391

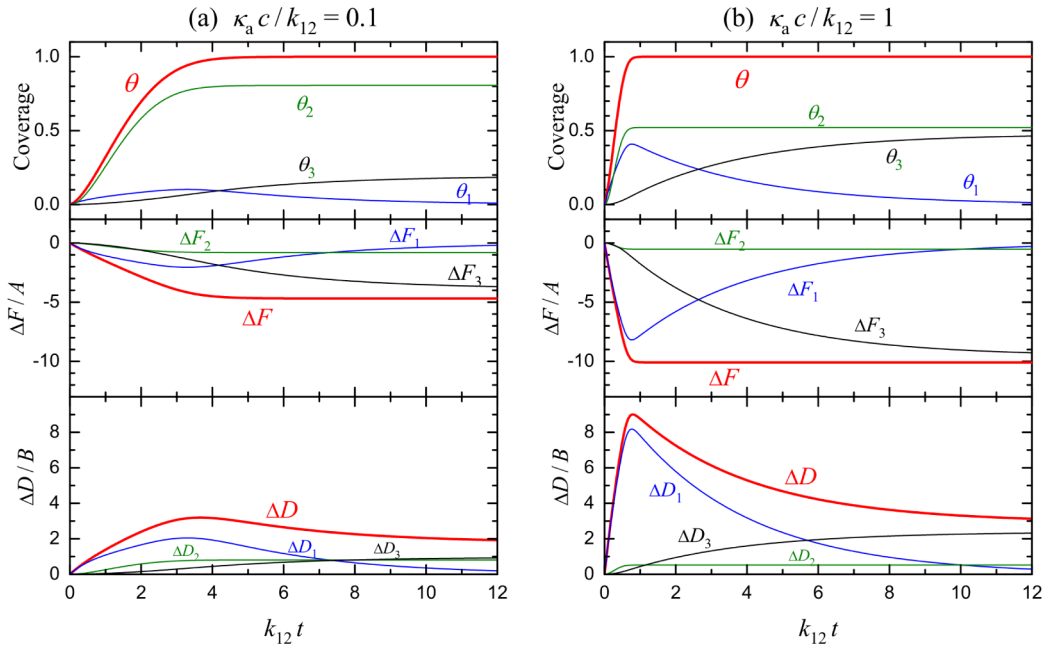


**Figure 5.** Mean-field adsorption kinetics predicted by the three-state model (eq 2) taking monomolecular relaxation of peptides into account. The total and partial coverages, $\theta$, $\theta_1$, $\theta_2$, $\theta_3$, and QCM-D signals (eq 5) are shown as a function of $k_{12}t$ for $\kappa_a c/k_{12} = 0.1$ (a) and 1 (b). The parameters employed in the calculations are as follows: $k_{13} = 0.3k_{12}$, $\theta_* = 0.9$, $\alpha = 10$, $\beta_1 = 20$, $\beta_3 = \beta_1$ (or $A_3 = A_1$), $\gamma_1 = 20$, and $\gamma_3 = 5$. The parameters for the contribution of peptides in state 3 to the QCM-D signals are chosen such that the partial contribution (per peptide) to $\Delta F$ is the same as in state 1 whereas the partial contribution to $\Delta D$ is smaller than in state 1. With this specification, the transition from state 1 to state 3 results in the drop of $\Delta D$ (after reaching a maximum) but does not influence $\Delta F$.

$$k_a = \frac{\kappa_a}{1 + (1 - \theta_*)/(1 - \theta)} \tag{3}$$

where $\kappa_a$ is the coverage-independent attachment rate constant below saturation, and $\theta_*$ is the coverage (close to unity, e.g., $\simeq$ 0.9) corresponding to the transition from the diffusion-limited regime to the kinetically-limited regime near saturation (the accurate calculation of $\theta_*$ is challenging[70] and beyond the scope of this paper).

In the mean-field approximation, the experimentally measured QCM-D responses are related to the peptide surface concentrations as

$$\Delta F = -A_1 c_1 - A_2 c_2 - A_3 c_3 \text{ and } \Delta D = B_1 c_1 + B_2 c_2 + B_3 c_3 \tag{4}$$

where $A_1$, $A_2$, $A_3$, $B_1$, $B_2$, and $B_3$ are the sensitivity constants. Employing (1) with $s_3 = s_1$, these expressions can be rewritten in terms of coverages,

$$\Delta F = -A(\beta_1\theta_1 + \theta_2 + \beta_3\theta_3) \text{ and } \Delta D = B(\gamma_1\theta_1 + \theta_2 + \gamma_3\theta_3) \tag{5}$$

where $A \equiv A_2/s_2$, $\beta_1 = \alpha A_1/A_2$, $\beta_3 = \alpha A_3/A_2$, $B \equiv B_2/s_2$, $\gamma_1 = \alpha B_1/B_2$, and $\gamma_3 = \alpha B_3/B_2$.

The model outlined above describes qualitatively the features of the observed adsorption kinetics of the peptides under consideration. With increasing adsorption rate, it predicts transition from the formation of the overlayer in state 2 at relatively low adsorption rates ($\kappa_a c/k_{12} \ll 1$) to the formation of the overlayer in state 1 at relatively high adsorption rates ($\kappa_a c/k_{12} \gg 1$). In these limits, the kinetics are predicted to be nearly monotonous (see, e.g., Figure 5a). At intermediate adsorption rates, the kinetics may be nonmonotonous (see, e.g., Figure 5b) as observed in the AH2 case.

Of note, we may add that the parameters employed in calculations have been chosen to describe the scale of the QCM-D signals observed with increasing the peptide concentration by one order of magnitude in the most interesting case of AH2 (Figure 4). In fact, we use dimensionless parameters or combinations of the parameters. In the context of kinetics, the most important one, $k_{12}/\kappa_a c$, is considered to vary in a wide range in order to describe various kinetic regimes. What might be unusual at first sight is that $\alpha$ is considered to be large. Physically, this appears to reflect that the peptide−lipid-bilayer contact area is in state 2 appreciably larger than that in state 1. This is possible e.g., if state 1 corresponds to the brush-like arrangement of peptides whereas state 2 is associated with the arrangement with the full contact with the SLB, so that the peptide−SLB contact area per peptide in the state with full contact (state 2) is much larger than in the brush-like state (state 1). $\beta_1$, $\beta_3$, $\gamma_1$, and $\gamma_3$ are proportional to $\alpha$ and large as well. In other words, the latter parameters are large due to their association with the expression the QCM-D signals via coverages (eq 5). Thus, the values of $\alpha$, $\beta_1$, $\beta_3$, $\gamma_1$, and $\gamma_3$ have been selected consistently.

In a more general context, one is expected to see fitting the experimentally measured kinetics by using a model. In the case of the mean-field models aimed at biomolecules, this is often hardly possible because (i) the understanding of the underlying factors is limited and (ii) the accuracy of the mean-field approximation is limited as well. For example, the mean-field models describing protein adsorption accompanied by relaxation of their shape are long available,[1,2] but the cases of their use for quantitative fitting are still limited despite the


https://doi.org/10.1021/acs.langmuir.6c02775
Langmuir 2026, 42, 32381−32391

Downloaded from pubs.acs.org/langd5/article-pdf/42/44/32381/6860487/acs.langmuir.6c02775.pdf by NANYANG TECHNOLOGICAL UNIV user on 19 November 2026

abundance of the related experimental data. Anyway, however, the models are highly useful at least at the conceptual level.

With the reservation above, we may notice that the type of the kinetics predicted by our model is shown in detail in Figure 5 and in the Supporting Information. Comparing them with the kinetics of adsorption of the peptides under consideration (Figure 4), one can easily conclude that quantitative fitting is possible in the AH case. The shape of the experimentally observed kinetics in the AH1 and AH2 cases is more complex, and accurate quantitative fitting is hardly possible. Under such circumstances, the explicit fitting will hardly add something really new and may only obscure the main message. Despite this remark, we believe that the fact that our model has allowed us to qualitatively interpret complex $\Delta F$- and $\Delta D$-tracked kinetics, and to introduce the dimensionless parameters $k_{12}/\kappa_a c$ and $\gamma_1$ for the classification of the observed kinetics, is encouraging.

## CONCLUSION

In this study, we have combined concentration-dependent QCM-D measurements with a phenomenological kinetic framework to elucidate the sequence-encoded membrane binding dynamics of three amphipathic helices derived from HCV nonstructural proteins. By applying a unified three-state adsorption−relaxation model, we demonstrate that these helices do not require distinct mechanistic descriptions; instead, their kinetic divergence arises from different values of a common set of dimensionless parameters governing attachment, aggregation, and structural relaxation. NS5A AH occupies the insertion-dominant regime characterized by rapid relaxation (large $k_{12}/\kappa_a c$), negligible mechanical contrast ($\beta_1 \approx 1, \gamma_1 \approx 1$), and near-Langmuirian monotonic adsorption. NS4B AH1 resides in an intermediate regime where moderate relaxation rates and finite mechanical contrast permit limited transient aggregation without triggering a concentration-dependent transition. In contrast, NS4B AH2 operates in an aggregation-dominant regime at low surface coverage, where smaller effective relaxation rates and large viscoelastic contrast factors allow accumulation of disordered, hydrated domains prior to cooperative compaction into membrane-engaged structures at higher coverage.

The strong concentration dependence observed for AH2 reflects nonequilibrium interfacial dynamics driven by slow structural relaxation under spatial constraints. This behavior cannot be captured by classical one-state adsorption models and instead requires a coupled adsorption−aggregation−reorganization framework. Importantly, the model parameters extracted from QCM-D fitting provide a quantitative kinetic description in which each helix is characterized by a distinct relaxation rate and mechanical contrast. In this context, it is of interest to add that the important role of slow relaxation of condensed matter during e.g., adsorption of polymers at appreciable coverage or growth of a new phase e.g., during molecular-beam epitaxy is now recognized and appreciated (see, e.g., refs 71 and 72, respectively). Such processes are expected to be significant in the case of adsorption of large biological molecules as well. Our observations for NS4B AH2 appear to be a good example of this category for membrane binding kinetics of AH peptides.

These findings establish that viral amphipathic helices are not functionally interchangeable membrane anchors. Rather, subtle sequence variations tune the balance between helix−membrane and helix−helix interactions, thereby controlling the accessible kinetic regime and mechanical outcome at the membrane interface. More broadly, this work advances a surface-science perspective on membrane-active helices, demonstrating that primary sequence encodes not only binding affinity but also dynamic pathway selection. Of note, the observed peptide adsorption kinetics are more complex compared to conventional protein adsorption kinetics. Overall, the framework presented here provides a generalizable basis for rational design of concentration-sensitive interfacial peptides and for interpreting complex adsorption kinetics beyond the Langmuir paradigm.

## ASSOCIATED CONTENT

### Supporting Information

The Supporting Information is available free of charge at https://pubs.acs.org/doi/10.1021/acs.langmuir.6c02775.

Detailed description of two mean-field three-state kinetic models of peptide adsorption and additional QCM-D data (PDF)

## AUTHOR INFORMATION


### Corresponding Author

**Nam-Joon Cho** − *School of Materials Science and Engineering, Nanyang Technological University, Singapore 637553, Singapore; Centre for Cross Economy Global, Nanyang Technological University, Singapore 637551, Singapore;* orcid.org/0000-0002-8692-8955; Email: njcho@ntu.edu.sg

### Authors

**Young Hwan Choe** − *School of Materials Science and Engineering, Nanyang Technological University, Singapore 637553, Singapore; Centre for Cross Economy Global, Nanyang Technological University, Singapore 637551, Singapore*

**Enzo Ng** − *School of Materials Science and Engineering, Nanyang Technological University, Singapore 637553, Singapore; Centre for Cross Economy Global, Nanyang Technological University, Singapore 637551, Singapore;* orcid.org/0009-0009-0760-9146

**Vladmir P. Zhdanov** − *Boreskov Institute of Catalysis, Russian Academy of Sciences, Novosibirsk 630090, Russia;* orcid.org/0000-0002-0167-8783

**Dongping Jiang** − *School of Materials Science and Engineering, Nanyang Technological University, Singapore 637553, Singapore; Centre for Cross Economy Global, Nanyang Technological University, Singapore 637551, Singapore*

Complete contact information is available at: https://pubs.acs.org/10.1021/acs.langmuir.6c02775


### Notes

The authors declare no competing financial interest.

## ACKNOWLEDGMENTS

This work was supported by Nanyang Technological University, Singapore, and funded by the Ministry of Education (MOE), Singapore, under the Academic Research Fund Tier 3 (Award No. MOET32022-0002), and by the National Research Foundation, Prime Minister's Office, Singapore, through its Campus for Research Excellence and

Downloaded from pubs.acs.org/langds/article-pdf/42/44/32381/6860487/acs.langmuir.6c02775.pdf by NANYANG TECHNOLOGICAL UNIV user on 19 November 2026

Technological Enterprise (CREATE) program via the Cellular Agriculture (CellAg) Program (Grant No. 370184512). The authors thank colleagues from the Translational Science for Sustainable Materials (TSSM) and the Centre for Cross Economy (CCE), NTU, for their valuable insights.

## REFERENCES

(1) Rabe, M.; Verdes, D.; Seeger, S. Understanding protein adsorption phenomena at solid surfaces. *Adv. Colloid Interface Sci.* **2011**, *162* (1), 87−106.
(2) Kim, J. Mathematical modeling approaches to describe the dynamics of protein adsorption at solid interfaces. *Colloids Surf., B* **2018**, *162*, 370−379.
(3) Quan, X.; Liu, J.; Zhou, J. Multiscale modeling and simulations of protein adsorption: progresses and perspectives. *Curr. Opin. Colloid Interface Sci.* **2019**, *41*, 74−85.
(4) Cho, N.-J.; Cheong, K. H.; Lee, C.; Frank, C. W.; Glenn, J. S. Binding Dynamics of Hepatitis C Virus' NS5A Amphipathic Peptide to Cell and Model Membranes. *J. Virol.* **2007**, *81* (12), 6682−6689.
(5) John, T.; Greene, G. W.; Patil, N. A.; Dealey, T. J. A.; Hossain, M. A.; Abel, B.; Martin, L. L. Adsorption of Amyloidogenic Peptides to Functionalized Surfaces Is Biased by Charge and Hydrophilicity. *Langmuir* **2019**, *35* (45), 14522−14531.
(6) Yang, Y.; Huang, J.; Dornbusch, D.; Grundmeier, G.; Fahmy, K.; Keller, A.; Cheung, D. L. Effect of Surface Hydrophobicity on the Adsorption of a Pilus-Derived Adhesin-like Peptide. *Langmuir* **2022**, *38* (30), 9257−9265.
(7) Teixeira, M. A.; Murthy, N. S.; Ferreira, D. P.; Felgueiras, H. P. Comparison of the adsorption of linear and cyclic antimicrobial peptides onto cellulosic compounds-reinforced poly(vinyl alcohol) films using QCM-D. *Colloids Surf., A* **2024**, *687*, 133490.
(8) Michaelis, M.; Limo, M. J.; Kothur, S. R.; Perry, C. C. Platinum-Binding Peptides: Binding Kinetics, Affinities, and Facet-Specific Conformational Adaptation. *Eur. J. Inorg. Chem.* **2025**, *28* (27), No. e202500224.
(9) Enkavi, G.; Javanainen, M.; Kulig, W.; Róg, T.; Vattulainen, I. Multiscale Simulations of Biological Membranes: The Challenge To Understand Biological Phenomena in a Living Substance. *Chem. Rev.* **2019**, *119* (9), 5607−5774.
(10) Steinkühler, J.; Lipowsky, R.; Miettinen, M. S. Molecular Dynamics Simulations Show That Short Peptides Can Drive Synthetic Cell Division by Binding to the Inner Membrane Leaflet. *J. Phys. Chem. B* **2024**, *128* (36), 8782−8787.
(11) Khodam Hazrati, M.; Vácha, R. Membrane Adsorption Enhances Translocation of Antimicrobial Peptide Buforin 2. *J. Phys. Chem. B* **2024**, *128* (35), 8469−8476.
(12) Zhdanov, V. P. Interaction of amphipathic α-helical peptides with a lipid membrane: Adsorption and pore formation. *Phys. A: Stat. Mech. Appl.* **2014**, *401*, 45−51.
(13) Giménez-Andrés, M.; Čopič, A.; Antonny, B. The Many Faces of Amphipathic Helices. *Biomolecules* **2018**, *8* (3), 45.
(14) Zimmerberg, J.; Kozlov, M. M. How proteins produce cellular membrane curvature. *Nat. Rev. Mol. Cell Biol.* **2006**, *7* (1), 9−19.
(15) Baumgart, T.; Capraro, B. R.; Zhu, C.; Das, S. L. Thermodynamics and Mechanics of Membrane Curvature Generation and Sensing by Proteins and Lipids. *Annu. Rev. Phys. Chem.* **2011**, *62*, 483−506.
(16) Fowler, P. W.; Hélie, J.; Duncan, A.; Chavent, M.; Koldsø, H.; Sansom, M. S. P. Membrane stiffness is modified by integral membrane proteins. *Soft Matter* **2016**, *12* (37), 7792−7803.
(17) Zemel, A.; Ben-Shaul, A.; May, S. Modulation of the Spontaneous Curvature and Bending Rigidity of Lipid Membranes by Interfacially Adsorbed Amphipathic Peptides. *J. Phys. Chem. B* **2008**, *112* (23), 6988−6996.
(18) Stumpf, B. H.; Nowakowski, P.; Eggeling, C.; Maciołek, A.; Smith, A.-S. Protein induced lipid demixing in homogeneous membranes. *Phys. Rev. Res.* **2021**, *3* (4), L042013.
(19) Khelashvili, G.; Harries, D.; Weinstein, H. Modeling Membrane Deformations and Lipid Demixing upon Protein-Membrane Interaction: The BAR Dimer Adsorption. *Biophys. J.* **2009**, *97* (6), 1626−1635.
(20) Schmidt, J. H.; Herlo, R.; Rombach, J.; Larsen, A. H.; Stoklund, M.; Perslev, M.; Nielsen, T. T. E.; Andersen, K. A.; Herenbrink, C. K.; Lycas, M. D.; et al. Membrane curvature association of amphipathic helix 8 drives constitutive endocytosis of GPCRs. *Sci. Adv.* **2025**, *11* (33), No. eadv1499.
(21) Laguera, B.; Golden, M. M.; Wang, F.; Gnewou, O.; Tuachi, A.; Egelman, E. H.; Wuest, W. M.; Conticello, V. P. Amphipathic Antimicrobial Peptides Illuminate a Reciprocal Relationship Between Self-assembly and Cytolytic Activity. *Angew. Chem., Int. Ed.* **2025**, *64* (21), No. e202500040.
(22) Cho, N.-J.; Lee, C.; Pang, P. S.; Pham, E. A.; Fram, B.; Nguyen, K.; Xiong, A.; Sklan, E. H.; Elazar, M.; Koytak, E. S.; Kersten, C.; Kanazawa, K. K.; Frank, C. W.; Glenn, J. S. Phosphatidylinositol 4,5-Bisphosphate Is an HCV NS5A Ligand and Mediates Replication of the Viral Genome. *Gastroenterology* **2015**, *148* (3), 616−625.
(23) Cho, N.-J.; Dvory-Sobol, H.; Lee, C.; Cho, S.-J.; Bryson, P.; Masek, M.; Elazar, M.; Frank, C. W.; Glenn, J. S. Identification of a Class of HCV Inhibitors Directed Against the Nonstructural Protein NS4B. *Sci. Transl. Med.* **2010**, *2* (15), 15ra6.
(24) Bryson, P. D.; Cho, N.-J.; Einav, S.; Lee, C.; Tai, V.; Bechtel, J.; Sivaraja, M.; Roberts, C.; Schmitz, U.; Glenn, J. S. A small molecule inhibits HCV replication and alters NS4B's subcellular distribution. *Antiviral Res.* **2010**, *87* (1), 1−8.
(25) Egger, D.; Wölk, B.; Gosert, R.; Bianchi, L.; Blum, H. E.; Moradpour, D.; Bienz, K. Expression of Hepatitis C Virus Proteins Induces Distinct Membrane Alterations Including a Candidate Viral Replication Complex. *J. Virol.* **2002**, *76* (12), 5974−5984.
(26) Lee, H.; Shin, H.; Wimmer, E.; Paul, A. V. *cis*-Acting RNA Signals in the NS5B C-Terminal Coding Sequence of the Hepatitis C Virus Genome. *J. Virol.* **2004**, *78* (20), 10865−10877.
(27) Tellinghuisen, T. L.; Marcotrigiano, J.; Rice, C. M. Structure of the zinc-binding domain of an essential component of the hepatitis C virus replicase. *Nature* **2005**, *435* (7040), 374−379.
(28) Love, R. A.; Brodsky, O.; Hickey, M. J.; Wells, P. A.; Cronin, C. N. Crystal Structure of a Novel Dimeric Form of NS5A Domain I Protein from Hepatitis C Virus. *J. Virol.* **2009**, *83* (9), 4395−4403.
(29) Drin, G.; Antonny, B. Amphipathic helices and membrane curvature. *FEBS Lett.* **2010**, *584* (9), 1840−1847.
(30) Hristova, K.; Wimley, W. C.; Mishra, V. K.; Anantharamiah, G. M.; Segrest, J. P.; White, S. H. An amphipathic α-helix at a membrane interface: a structural study using a novel X-ray diffraction method. *J. Mol. Biol.* **1999**, *290* (1), 99−117.
(31) Penna, M. J.; Mijajlovic, M.; Tamerler, C.; Biggs, M. J. Molecular-level understanding of the adsorption mechanism of a graphite-binding peptide at the water/graphite interface. *Soft Matter* **2015**, *11* (26), 5192−5203.
(32) Penna, M. J.; Mijajlovic, M.; Biggs, M. J. Molecular-Level Understanding of Protein Adsorption at the Interface between Water and a Strongly Interacting Uncharged Solid Surface. *J. Am. Chem. Soc.* **2014**, *136* (14), 5323−5331.
(33) Ben Amor, N.; Bauer, D.; Braconnier, B.; Coasne, B. Adsorption Thermodynamics and Kinetics of Simple and Complex Fluids: Physical Modeling of Surface Saturation, Reservoir Depletion, Lateral Interactions, and Collective Effects. *Langmuir* **2026**, *42* (1), 1348−1357.
(34) Yu, Q.; Košmrlj, A. Pattern formation of lipid domains in bilayer membranes. *Soft Matter* **2025**, *21* (21), 4288−4297.
(35) Ackerman, D. G.; Feigenson, G. W. Effects of Transmembrane α-Helix Length and Concentration on Phase Behavior in Four-Component Lipid Mixtures: A Molecular Dynamics Study. *J. Phys. Chem. B* **2016**, *120* (17), 4064−4077.
(36) Cebecauer, M.; Amaro, M.; Jurkiewicz, P.; Sarmento, M. J.; Šachl, R.; Cwiklik, L.; Hof, M. Membrane Lipid Nanodomains. *Chem. Rev* **2018**, *118* (23), 11259−11297.

Downloaded from pubs.acs.org/langds/article-pdf/42/44/32381/6860487/acs.langmuir.6c02775.pdf by NANYANG TECHNOLOGICAL UNIV user on 19 November 2026


https://doi.org/10.1021/acs.langmuir.6c02775
Langmuir 2026, 42, 32381−32391

(37) Stevens, M. J. Complementary Matching in Domain Formation within Lipid Bilayers. *J. Am. Chem. Soc.* **2005**, *127* (44), 15330−15331.
(38) Punia, R.; Goel, G. Free Energy Surface and Molecular Mechanism of Slow Structural Transitions in Lipid Bilayers. *J. Chem. Theory Comput.* **2023**, *19* (22), 8245−8257.
(39) Nanda, H.; García Sakai, V.; Khodadadi, S.; Tyagi, M. S.; Schwalbach, E. J.; Curtis, J. E. Relaxation dynamics of saturated and unsaturated oriented lipid bilayers. *Soft Matter* **2018**, *14* (29), 6119−6127.
(40) Yurtsever, A.; Sun, L.; Hirata, K.; Fukuma, T.; Rath, S.; Zareie, H.; Watanabe, S.; Sarikaya, M. Molecular Scale Structure and Kinetics of Layer-by-Layer Peptide Self-Organization at Atomically Flat Solid Surfaces. *ACS Nano* **2023**, *17* (8), 7311−7325.
(41) Zhdanov, V. P.; Kasemo, B. Monte Carlo Simulations of the Kinetics of Protein Adsorption. *Surf. Rev. Lett.* **1998**, *5* (2), 615−634.
(42) Holmberg, M.; Hou, X. Competitive Protein Adsorption—Multilayer Adsorption and Surface Induced Protein Aggregation. *Langmuir* **2009**, *25* (4), 2081−2089.
(43) Krug, J. Origins of scale invariance in growth processes. *Adv. Phys.* **1997**, *46* (2), 139−282.
(44) Tae, H.; Park, S.; Choe, Y.; Yang, C.; Cho, N.-J. Exploring the Interfacial Dynamics of Unilamellar and Multilamellar Cationic Liposomes on SiO2 and Their Interactions with Membrane-Active Peptide. *Langmuir* **2024**, *40* (47), 24761−24770.
(45) Johannsmann, D. Studies of Viscoelasticity with the QCM. In *Piezoelectric Sensors*; Steinem, C.; Janshoff, A. ed., Springer: Berlin, 2007, pp. 49−109
(46) Cho, N.-J.; Kanazawa, K. K.; Glenn, J. S.; Frank, C. W. Employing Two Different Quartz Crystal Microbalance Models To Study Changes in Viscoelastic Behavior upon Transformation of Lipid Vesicles to a Bilayer on a Gold Surface. *Anal. Chem.* **2007**, *79* (18), 7027−7035.
(47) Rodahl, M.; Höök, F.; Fredriksson, C. A.; Keller, C.; Krozer, A.; Brzezinski, P.; Voinova, M.; Kasemo, B. Simultaneous frequency and dissipation factor QCM measurements of biomolecular adsorption and cell adhesion. *Faraday Discuss* **1997**, *107*, 229−246.
(48) Du, B.; Johannsmann, D. Operation of the Quartz Crystal Microbalance in Liquids: Derivation of the Elastic Compliance of a Film from the Ratio of Bandwidth Shift and Frequency Shift. *Langmuir* **2004**, *20* (7), 2809−2812.
(49) Kiyota, T.; Lee, S.; Sugihara, G. Design and Synthesis of Amphiphilic α-Helical Model Peptides with Systematically Varied Hydrophobic−Hydrophilic Balance and Their Interaction with Lipid- and Bio-Membranes. *Biochemistry* **1996**, *35* (40), 13196−13204.
(50) Wimley, W. C.; White, S. H. Experimentally determined hydrophobicity scale for proteins at membrane interfaces. *Nat. Struct. Biol.* **1996**, *3* (10), 842−848.
(51) Snider, C.; Jayasinghe, S.; Hristova, K.; White, S. H. MPEx: A tool for exploring membrane proteins. *Protein Sci.* **2009**, *18* (12), 2624−2628.
(52) Combet, C.; Blanchet, C.; Geourjon, C.; Deléage, G. NPS@: Network Protein Sequence Analysis. *Trends Biochem. Sci.* **2000**, *25* (3), 147−150.
(53) Jackman, J. A.; Costa, V. V.; Park, S.; Real, A. L. C. V.; Park, J. H.; Cardozo, P. L.; Ferhan, A. R.; Olmo, I. G.; Moreira, T. P.; Bambirra, J. L.; Queiroz, V. F.; Queiroz-Junior, C. M.; Foureaux, G.; Souza, D. G.; Ribeiro, F. M.; Yoon, B. K.; Wynendaele, E.; De Spiegeleer, B.; Teixeira, M. M.; Cho, N.-J. Therapeutic treatment of Zika virus infection using a brain-penetrating antiviral peptide. *Nat. Mater.* **2018**, *17* (11), 971−977.
(54) Cho, N.-J.; Cho, S.-J.; Cheong, K. H.; Glenn, J. S.; Frank, C. W. Employing an Amphipathic Viral Peptide to Create a Lipid Bilayer on Au and TiO2. *J. Am. Chem. Soc.* **2007**, *129* (33), 10050−10051.
(55) Cho, N.-J.; Dvory-Sobol, H.; Xiong, A.; Cho, S.-J.; Frank, C. W.; Glenn, J. S. Mechanism of an Amphipathic α-Helical Peptide's Antiviral Activity Involves Size-Dependent Virus Particle Lysis. *ACS Chem. Biol.* **2009**, *4* (12), 1061−1067.
(56) Voinova, M. V.; Jonson, M.; Kasemo, B. 'Missing mass' effect in biosensor's QCM applications. *Biosens. Bioelectron.* **2002**, *17* (10), 835−841.
(57) Sauerbrey, G. Verwendung von Schwingquarzen zur Wägung dünner Schichten und zur Mikrowägung. *Z. Phys.* **1959**, *155* (2), 206−222.
(58) Eisenberg, D.; Weiss, R. M.; Terwilliger, T. C. The helical hydrophobic moment: a measure of the amphiphilicity of a helix. *Nature* **1982**, *299* (5881), 371−374.
(59) Gautier, R.; Douguet, D.; Antonny, B.; Drin, G. HELIQUEST: a web server to screen sequences with specific α-helical properties. *Bioinformatics* **2008**, *24* (18), 2101−2102.
(60) Yau, W.-M.; Wimley, W. C.; Gawrisch, K.; White, S. H. The Preference of Tryptophan for Membrane Interfaces. *Biochemistry* **1998**, *37* (42), 14713−14718.
(61) Jackman, J. A.; Saravanan, R.; Zhang, Y.; Tabaei, S. R.; Cho, N.-J. Correlation between Membrane Partitioning and Functional Activity in a Single Lipid Vesicle Assay Establishes Design Guidelines for Antiviral Peptides. *Small* **2015**, *11* (20), 2372−2379.
(62) Mills, F. D.; Antharam, V. C.; Ganesh, O. K.; Elliott, D. W.; McNeill, S. A.; Long, J. R. The Helical Structure of Surfactant Peptide KL4 When Bound to POPC: POPG Lipid Vesicles. *Biochemistry* **2008**, *47* (32), 8292−8300.
(63) Wimley, W. C.; Creamer, T. P.; White, S. H. Solvation Energies of Amino Acid Side Chains and Backbone in a Family of Host−Guest Pentapeptides. *Biochemistry* **1996**, *35* (16), 5109−5124.
(64) White, S. H.; Wimley, W. C. Membrane Protein Folding And Stability: Physical Principles. *Annu. Rev. Biophys.* **1999**, *28*, 319−365.
(65) Dyson, H. J.; Wright, P. E. Intrinsically unstructured proteins and their functions. *Nat. Rev. Mol. Cell Biol.* **2005**, *6* (3), 197−208.
(66) McCubbin, G. A.; Praporski, S.; Piantavigna, S.; Knappe, D.; Hoffmann, R.; Bowie, J. H.; Separovic, F.; Martin, L. L. QCM-D fingerprinting of membrane-active peptides. *Eur. Biophys. J.* **2011**, *40* (4), 437−446.
(67) Penin, F.; Dubuisson, J.; Rey, F. A.; Moradpour, D.; Pawlotsky, J.-M. Structural biology of hepatitis C virus. *Hepatology* **2004**, *39* (1), 5−19.
(68) Romero-Brey, I.; Bartenschlager, R. Endoplasmic Reticulum: The Favorite Intracellular Niche for Viral Replication and Assembly. *Viruses* **2016**, *8* (6), 160.
(69) Criscitiello, M. F.; de Figueiredo, P. Fifty Shades of Immune Defense. *PLoS Pathog.* **2013**, *9* (2), No. e1003110.
(70) Zhdanov, V. P.; Keller, C. A.; Glasmästar, K.; Kasemo, B. Simulation of adsorption kinetics of lipid vesicles. *J. Chem. Phys.* **2000**, *112* (2), 900−909.
(71) Thoms, E.; Song, Z.; Wang, K.; Napolitano, S. Simple Model to Predict the Adsorption Rate of Polymer Melts. *Phys. Rev. Lett.* **2024**, *132* (24), 248101.
(72) Lapkin, D.; Carrasco, I. S. S.; Luukkonen, C. C.; Konovalov, O.; Hinderhofer, A.; Schreiber, F.; Reis, F. D. A. A.; Oettel, M. Nonmonotonic Roughness Evolution in Film Growth on Weakly Interacting Substrates. *Phys. Rev. Lett.* **2026**, *136* (7), 076202.

Downloaded from pubs.acs.org/langd5/article-pdf/42/44/32381/6860487/acs.langmuir.6c02775.pdf by NANYANG TECHNOLOGICAL UNIV user on 19 November 2026


https://doi.org/10.1021/acs.langmuir.6c02775
*Langmuir* 2026, 42, 32381−32391